

Nonequilibrium dynamical cluster theory

Naoto Tsuji,¹ Peter Barmettler,² Hideo Aoki,³ and Philipp Werner⁴

¹*Department of Physics, University of Tokyo, Tokyo 113-0033, Japan*

²*Département de Physique Théorique, Université de Genève, 1211 Genève, Switzerland*

³*Department of Physics, University of Tokyo, 113-0033 Tokyo, Japan*

⁴*Department of Physics, University of Fribourg, 1700 Fribourg, Switzerland*

(Dated: August 22, 2021)

We study the effect of spatially nonlocal correlations on the nonequilibrium dynamics of interacting fermions by constructing the nonequilibrium dynamical cluster theory, a cluster generalization of the nonequilibrium dynamical mean-field theory (DMFT). The formalism is applied to interaction quenches in the Hubbard model in one and two dimensions, and the results are compared with data from single-site DMFT, the time-dependent density matrix renormalization group, and lattice perturbation theory. Both in one and two dimensions the double occupancy quickly thermalizes, while the momentum distribution relaxes only on much longer time scales. For the two-dimensional square lattice we find a strongly momentum-dependent evolution of the momentum distribution around the Fermi energy, with a much faster relaxation near the momenta $(0, \pi)$ and $(\pi, 0)$ than near $(\pi/2, \pi/2)$. This result is interpreted as reflecting the momentum-anisotropic quasiparticle lifetime of the marginal Fermi liquid. The method is further applied to the two-dimensional Hubbard model driven by a dc electric field, where the damping of the Bloch oscillation of the current is found to be less effective than predicted by DMFT and lattice perturbation theory.

PACS numbers: 71.10.Fd, 67.85.-d

I. INTRODUCTION

Simulating the nonequilibrium dynamics of microscopic models for quantum many-body systems is a great computational challenge,¹ but such calculations may provide new insights into the role of strong correlations in high-temperature superconductors and other correlated systems by disentangling complex fluctuations along the real-time axis. So far, various approaches have been proposed. One focus has been on one-dimensional (1D) systems, for which the time-dependent density matrix renormalization group (DMRG)²⁻⁴ and its variants have provided accurate results for the real-time evolution. Another approach comes from the opposite limit of infinite dimensions,⁵ where the nonequilibrium dynamical mean-field theory (DMFT),⁶⁻⁹ which incorporates temporal fluctuations but approximates the self-energy as a spatially local function, becomes an exact scheme. However, the nonequilibrium properties of quantum systems in two dimensions, which lies in between these two extremes, remain far from being theoretically understood.

From an experimental point of view, too, the dynamics of two-dimensional (2D) quantum systems is of particular interest. Recent time- and angle-resolved photoemission spectroscopy (ARPES) experiments start to reveal temporal evolutions of the occupation $n(\mathbf{k}, \omega, t)$ for correlated electrons in layered compounds.¹⁰⁻¹⁴ For example, it has been shown that the quasiparticle recombination in the d -wave superconductor $\text{Bi}_2\text{Sr}_2\text{CaCu}_2\text{O}_{8+\delta}$ occurs faster away from the “nodal line” ($k_x = \pm k_y$) in the Brillouin zone than near the nodal line.¹⁴ This kind of momentum-dependent relaxation dynamics can be related to *nonlocal quantum correlations*, which should become essential in low-dimensional quantum systems. We can then pose the following questions: What role do nonlocal correlations play in low-dimensional correlated systems out of equilibrium? And how can we take account of these effects

systematically in real-time simulations?

Motivated by these questions, we present and test here a theoretical approach, namely the *nonequilibrium dynamical cluster theory*, which is the cluster extension of the nonequilibrium DMFT, or the nonequilibrium generalization of dynamical cluster theories.¹⁵ In the DMFT formulation, we map a lattice model to a single-site impurity embedded in a dynamical mean field, using the assumption of a local self-energy, thereby neglecting nonlocal dynamical fluctuations. In cluster formalisms, this restriction is overcome by mapping the system onto a finite-size cluster problem with a spatially correlated dynamical mean field.

We then apply this scheme to the interaction-quench problem in the Hubbard model in 1D and 2D, changing the strength of the interaction abruptly in time. In cold atoms, where effective interactions can be tuned using Feshbach resonances or by changing the depth of optical lattice potentials, quantum quenches have become a standard procedure to trigger nonequilibrium dynamics,¹⁶⁻¹⁹ and the problem has attracted broad theoretical interests.²⁰⁻²⁹ A naive expectation is that after the quench the system is highly excited and is characterized by a high effective temperature, so that the nonlocal correlations might be wiped out, as in equilibrium at high temperatures. However, we will show that in 2D the momentum distribution, after experiencing prethermalization,^{22,23,30} exhibits a *momentum-dependent relaxation dynamics*: the distribution relaxes to the thermal one faster in the antinodal region [around $(0, \pi)$ or $(\pi, 0)$ in the Brillouin zone] than in the nodal region [around $(\pi/2, \pi/2)$]. The momentum-dependent relaxation, observable only when we go from the single-site to the cluster formalism, comes from the nonlocal correlations. Our finding is consistent with the quasiparticle lifetime of the marginal Fermi liquid, which is highly anisotropic in momentum space.

We also examine a 1D system, where we can benchmark

the cluster calculations rigorously by comparing the time-evolution to numerically exact DMRG results, and test the convergence of the results with respect to the cluster size. Here, we find a rapid thermalization of the double occupancy similar to the 2D case, apart from additional oscillations due to divergences in the density of states at the band edges.

II. GENERAL FORMULATION

We will formulate the nonequilibrium dynamical cluster theory by taking the Hubbard model as an example. The time-dependent Hamiltonian is given by

$$H(t) = -J \sum_{\langle ij \rangle, \sigma} (c_{i\sigma}^\dagger c_{j\sigma} + \text{H.c.}) - \mu \sum_{i, \sigma} \hat{n}_{i\sigma} + U(t) \sum_i \hat{n}_{i\uparrow} \hat{n}_{i\downarrow},$$

where $c_{i\sigma}^\dagger$ creates a lattice fermion at the i th site with spin σ , $\hat{n}_{i\sigma} \equiv c_{i\sigma}^\dagger c_{i\sigma}$, J is the hopping amplitude, μ the chemical potential, U the (time-dependent) interaction strength, and the sum $\langle ij \rangle$ is taken over nearest-neighbor sites. There are two well-established constructions for the cluster mapping: the cellular DMFT^{31,32} and the dynamical cluster approximation (DCA).^{33,34} Here we adopt the DCA, since it preserves the periodicity of the lattice structure by construction. This enables us to use the diagonal (momentum) representation for the cluster Green's function, while in the cellular DMFT the cluster Green's function has to be represented in real space with off-diagonal elements. The cluster Dyson equation, which we shall introduce below, then becomes a "matrix" integral-differential equation, which is hard to solve for large size clusters [with the computational cost scaling as $O(N_c^3)$ for clusters of size N_c]. This is why we have here opted for the DCA.

The cluster reference system is defined by the action

$$\begin{aligned} \mathcal{S}_{\text{clust}}[\Delta] = & -J \int_{\mathcal{C}} dt \sum_{\langle ij \rangle, \sigma} d_{\mathbf{R}_i, \sigma}^\dagger(t) d_{\mathbf{R}_j, \sigma}(t) - \mu \int_{\mathcal{C}} dt \sum_{i\sigma} \hat{n}_{\mathbf{R}_i, \sigma}(t) \\ & + \int_{\mathcal{C}} dt U(t) \sum_i \hat{n}_{\mathbf{R}_i, \uparrow}(t) \hat{n}_{\mathbf{R}_i, \downarrow}(t) \\ & + \int_{\mathcal{C}} dt \int_{\mathcal{C}} dt' \sum_{ij\sigma} d_{\mathbf{R}_i, \sigma}^\dagger(t) \Delta_\sigma(\mathbf{R}_i - \mathbf{R}_j; t, t') d_{\mathbf{R}_j, \sigma}(t'), \end{aligned}$$

where $d_{\mathbf{R}, \sigma}^\dagger$ creates a cluster fermion at a cluster site \mathbf{R}_i , $\Delta_\sigma(\mathbf{R}; t, t')$ is the hybridization function that will be determined self-consistently, $\hat{n}_{\mathbf{R}\sigma} = d_{\mathbf{R}\sigma}^\dagger d_{\mathbf{R}\sigma}$, and the time integral is taken along the Kadanoff-Baym contour \mathcal{C} ,³⁵ running along $t = 0 \rightarrow t_{\text{max}} \rightarrow 0 \rightarrow -i\beta$ (where t_{max} is the maximum time up to which the system is evolved, and β the inverse temperature of the initial thermal state). With this action, we define the cluster Green's function $G_\sigma^{\text{clust}}(\mathbf{R} - \mathbf{R}'; t, t') = -i \langle \mathcal{T}_{\mathcal{C}} d_{\mathbf{R}\sigma}(t) d_{\mathbf{R}'\sigma}^\dagger(t') \rangle_{\mathcal{S}_{\text{clust}}}$ with $\mathcal{T}_{\mathcal{C}}$ the contour-ordering operator along \mathcal{C} and $\langle \dots \rangle_{\mathcal{S}_{\text{clust}}} = \text{Tr}(\mathcal{T}_{\mathcal{C}} e^{-i\mathcal{S}_{\text{clust}}} \dots) / \text{Tr}(\mathcal{T}_{\mathcal{C}} e^{-i\mathcal{S}_{\text{clust}}})$.

If we denote by \mathbf{K} the wave vector reciprocal to \mathbf{R} , we can write the Fourier-transformed cluster Green's function as

$$G_\sigma^{\text{clust}}(\mathbf{K}; t, t') = \sum_j e^{-i\mathbf{K} \cdot \mathbf{R}_j} G_\sigma^{\text{clust}}(\mathbf{R}_j; t, t').$$

The Brillouin zone is divided into N_c sectors, each of which is centered at the corresponding \mathbf{K} . There are various choices of clusters. We adopt two cases,

$$\begin{aligned} \text{A: } \mathbf{K}_{x,y} &= 2n_{x,y}\pi/N_c, \\ \text{B: } \mathbf{K}_{x,y} &= (2n_{x,y} - 1)\pi/N_c \end{aligned}$$

($n_{x,y}$: integers). In the lattice problem, an arbitrary wave vector \mathbf{k} can be written as $\mathbf{K} + \tilde{\mathbf{k}}$, where $\tilde{\mathbf{k}}$ represents the relative momentum from the center of the momentum sector. The mapping from the lattice to the cluster problem (i.e., the choice of the hybridization function Δ_σ) is defined such that the cluster Green's function is reproduced by the lattice Green's function averaged over the corresponding momentum sector,

$$G_\sigma^{\text{clust}}[\Delta](\mathbf{K}; t, t') = \frac{N_c}{N} \sum_{\tilde{\mathbf{k}}} G_\sigma^{\text{lat}}(\mathbf{K} + \tilde{\mathbf{k}}; t, t'),$$

with N the total number of k points. The Green's functions and self-energies are related via the cluster Dyson equation,

$$\begin{aligned} (i\partial_t + \mu)G_\sigma^{\text{clust}}(\mathbf{K}) - \Delta_\sigma(\mathbf{K}) * G_\sigma^{\text{clust}}(\mathbf{K}) - \Sigma_\sigma^{\text{clust}}(\mathbf{K}) * G_\sigma^{\text{clust}}(\mathbf{K}) \\ = \delta_{\mathcal{C}}(t, t'), \end{aligned}$$

with $*$ representing a convolution along the contour \mathcal{C} , and the lattice Dyson equation,

$$(i\partial_t + \mu)G_\sigma^{\text{lat}}(\mathbf{k}) - \epsilon(\mathbf{k}) * G_\sigma^{\text{lat}}(\mathbf{k}) - \Sigma_\sigma^{\text{lat}}(\mathbf{k}) * G_\sigma^{\text{lat}}(\mathbf{k}) = \delta_{\mathcal{C}}(t, t'),$$

where $\epsilon(\mathbf{k}) = -2J \sum_{i=1}^d \cos k_i$ is the band dispersion, and $\delta_{\mathcal{C}}(t, t')$ the contour delta function defined on \mathcal{C} . In the nonequilibrium DCA, we identify the lattice self-energy with the cluster self-energy,

$$\Sigma_\sigma^{\text{lat}}(\mathbf{K} + \tilde{\mathbf{k}}; t, t') = \Sigma_\sigma^{\text{clust}}(\mathbf{K}; t, t'),$$

that is, we neglect the $\tilde{\mathbf{k}}$ dependence of $\Sigma_\sigma^{\text{lat}}(\mathbf{K} + \tilde{\mathbf{k}}; t, t')$. In this way, the problem is reduced to solving the cluster problem, for which one may use several possible solvers developed for the nonequilibrium DMFT, e.g., the weak-coupling perturbation theory,^{36,37} quantum Monte Carlo,³⁸ the noncrossing approximation (NCA),³⁹ and exact-diagonalization-based approaches.^{40,41}

In the present formalism, spatial correlations are systematically included within a finite range cutoff $L \sim N_c^{1/d}$. In the large cluster-size limit ($N_c \rightarrow \infty$), the formalism should become exact in arbitrary dimensions. A virtue of the nonequilibrium DCA is that it provides a self-consistency scheme that updates the "noninteracting part" (Δ_σ) of the action, so that it can describe "thermalization" in the long-time limit. This discriminates it from other existing approaches that capture nonlocal correlations in the time evolution. For instance, the conventional lattice perturbation technique expands the self-energy in terms of the noninteracting lattice Green's function, so that the memory of the initial state is kept permanently. In cluster perturbation theory,⁴²⁻⁴⁴ which decomposes the system into clusters and treats the inter-cluster connections perturbatively, the feedback to the exactly solved subsystems is limited. The dual-fermion approach provides another

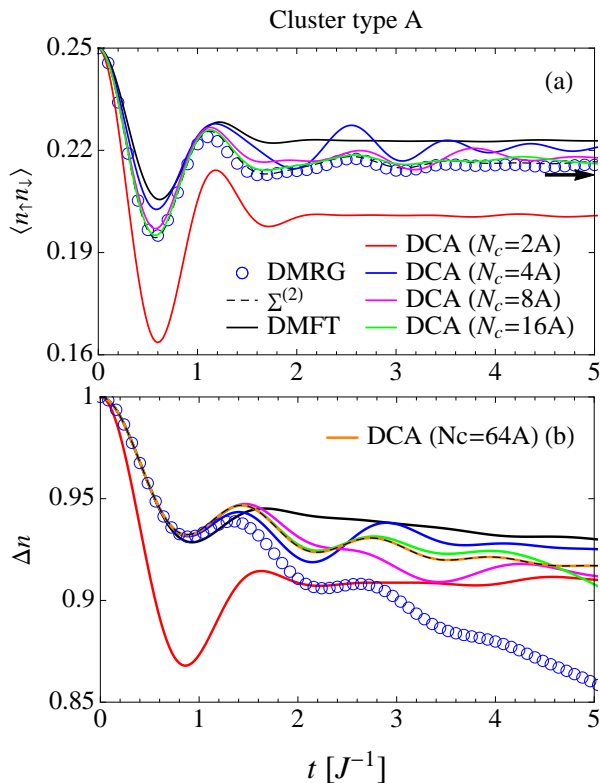


FIG. 1: (a) The double occupancy and (b) the jump in the momentum distribution for a quench $U/J = 0 \rightarrow 1$ in the 1D Hubbard model calculated by DCA with cluster type A, and compared with other methods. The arrow in (a) indicates the thermal value of the double occupancy evaluated from the finite-temperature DMRG.

path to extend the DMFT, but its application to nonequilibrium situations is so far limited to a small cluster and impurity problem.^{45,46} Very recently, the equation-of-motion method has been applied to the 2D Hubbard model.²⁹ This scheme allows to compute numerically exact results, but only up to relatively short times.

If we concentrate on the weak-coupling regime at half-filling, we can employ the iterative perturbation theory (IPT) as a cluster solver:

$$\Sigma_{\sigma}^{\text{clust}}(\mathbf{R}; t, t') = U(t)U(t')\mathcal{G}_{0\sigma}(\mathbf{R}; t, t')\mathcal{G}_{0\bar{\sigma}}(-\mathbf{R}; t', t)\mathcal{G}_{0\bar{\sigma}}(\mathbf{R}; t, t').$$

Here $\mathcal{G}_{0\sigma}(\mathbf{R}; t, t')$ is the cluster Weiss mean-field propagator defined by

$$(i\partial_t + \mu)\mathcal{G}_{0\sigma}(\mathbf{K}) - \Delta_{\sigma}(\mathbf{K}) * \mathcal{G}_{0\sigma}(\mathbf{K}) = \delta_{\mathcal{C}}(t, t').$$

We note that IPT as an impurity solver in nonequilibrium DMFT calculations works adequately for U smaller than or equal to half the bandwidth.³⁷

We can use the time-dependent DMRG²⁻⁴ to benchmark the DCA result for the 1D system. By using a matrix-product state formalism in the thermodynamic limit,⁴⁷ we can get rid of finite-size effects, with the accuracy of the results only limited by the number of DMRG states, which is chosen here to be $D = 800$ for the initial state and up to $D = 3600$ for the

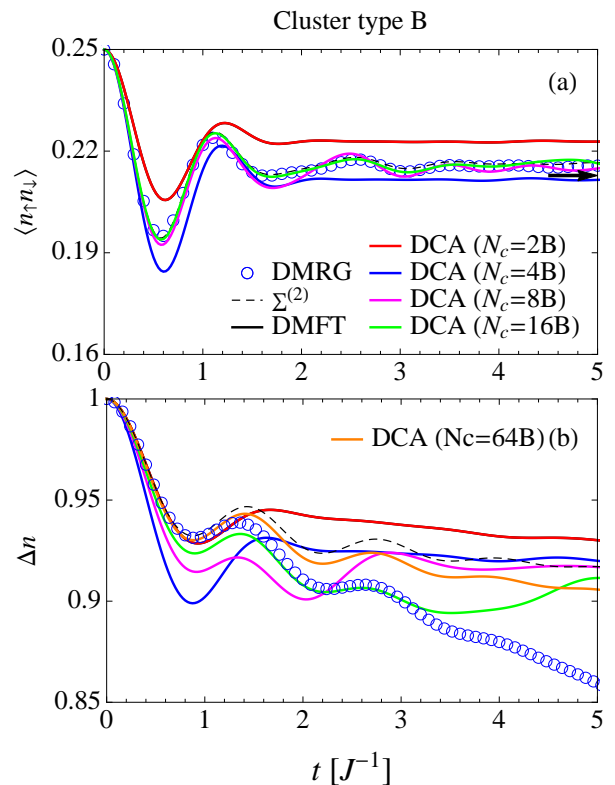


FIG. 2: (a) The double occupancy and (b) the jump in the momentum distribution for a quench $U/J = 0 \rightarrow 1$ in the 1D Hubbard model calculated by DCA with cluster type B, and compared with other methods. The arrow in (a) indicates the thermal value of the double occupancy evaluated from the finite-temperature DMRG.

subsequent time evolution. The maximum truncation of the density-matrix eigenvalues is $\epsilon = 10^{-7}$, leading to numerical errors much smaller than the symbol sizes in the figures. The initial state is generated by an imaginary-time evolution with an explicit orthogonalization scheme applied.⁴⁸ We have also performed finite-temperature DMRG⁴⁹⁻⁵¹ calculations to compare the long-time properties with thermal-equilibrium results.

III. INTERACTION QUENCH: 1D HUBBARD MODEL

As a first application, we study the interaction quench $U(t) = 0 \rightarrow U > 0$ for the Hubbard model, starting from the noninteracting zero-temperature state. We plot the time evolution of the double occupancy $d(t) = \langle \hat{n}_{\uparrow}(t)\hat{n}_{\downarrow}(t) \rangle$, along with the jump $\Delta n(t)$ in the momentum distribution $n(\mathbf{k}, t) = \langle c_{\mathbf{k}\sigma}^{\dagger}(t)c_{\mathbf{k}\sigma}(t) \rangle$ at the Fermi energy [$\epsilon(\mathbf{k}) = \epsilon_F$]. Figure 1 (Fig. 2) shows results for the 1D Hubbard model calculated by the DCA with cluster type A (B). We also plot for comparison the results of DMRG, DMFT, and the second-order lattice perturbation theory ($\Sigma^{(2)}$). The number of k points is $N = 1024$ for the methods other than DMRG. Compared to the infinite-coordination Bethe lattice, where $d(t)$ relaxes rapidly,²³ DMFT predicts a damped oscillation in $d(t)$ for the

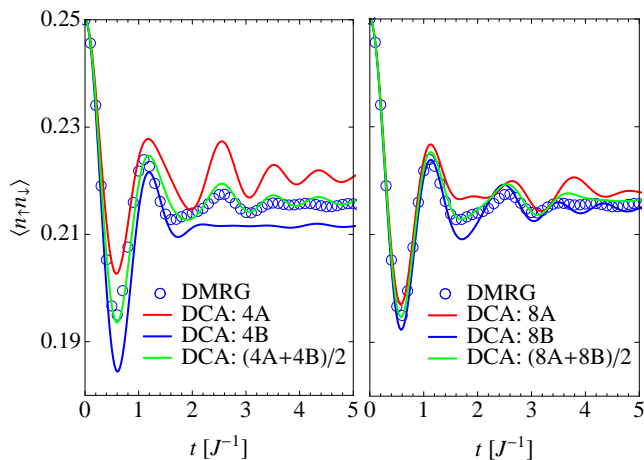


FIG. 3: Averaging of the double occupancy obtained by DCA with cluster types A (Fig. 1) and B (Fig. 2) for $N_c = 4$ (left) and $N_c = 8$ (right).

1D lattice. DCA with $N_c = 2B$ (i.e., $N_c = 2$ with cluster type B) is exactly equivalent to DMFT due to the Brillouin-zone symmetry [Fig. 2(a)], while the DCA result for $d(t)$ with $N_c = 2A$ is overall smaller than that of DMFT having a damped oscillation [Fig. 1(a)]. As we proceed to DCA with $N_c \geq 4$ where the momentum space near the Fermi energy and the band edge can be distinguished, the oscillations become more pronounced. This suggests that the oscillation originates from the divergence of the density of states at the band edges in 1D. In fact, the oscillation period is roughly $2\pi/(4J)$ (with $4J$ being the bandwidth of the 1D lattice). As N_c is increased, the cluster-type (A or B) dependence becomes weaker, and the DCA results converge to the exact DMRG. If we take an average of the results obtained from DCA over the cluster types A and B (Fig. 3), the convergence to DMRG in the limit of $N_c \rightarrow \infty$ is notably accelerated, with a fair agreement already seen even at $N_c = 4$.

Unlike the double occupancy, the jump in the momentum distribution Δn in DCA [Fig. 1(b) for cluster type A and Fig. 2(b) for type B] does not converge rapidly with N_c . This can be related to the nonlocal nature of the quantity Δn , which is derived via Fourier transformation from the real-space correlation $\langle c_{i\sigma}^{\dagger} c_{j\sigma} \rangle$. If we increase N_c up to 64, we observe that DCA+IPT approaches $\Sigma^{(2)}$ for the 1D case. The deviation from DMRG must be attributed to quantum corrections from higher-order diagrams neglected in IPT. According to DMFT, $\Delta n(t)$ exhibits a prethermalization plateau²³ after a rapid initial drop, which is a characteristic feature of prethermalization.^{22,52} According to DCA and DMRG, however, a clear prethermalization plateau is not observed. Instead, similar to $d(t)$, we see an oscillation in $\Delta n(t)$ which does not damp fast, unlike in the higher-dimensional cases. The momentum distribution relaxes much more slowly than $d(t)$, and is still far from the thermal distribution with $\Delta n = 0$ on the computationally accessible time scale.

While one might think that the 1D Hubbard model, being integrable,⁵³ should be prevented from thermalization, we find

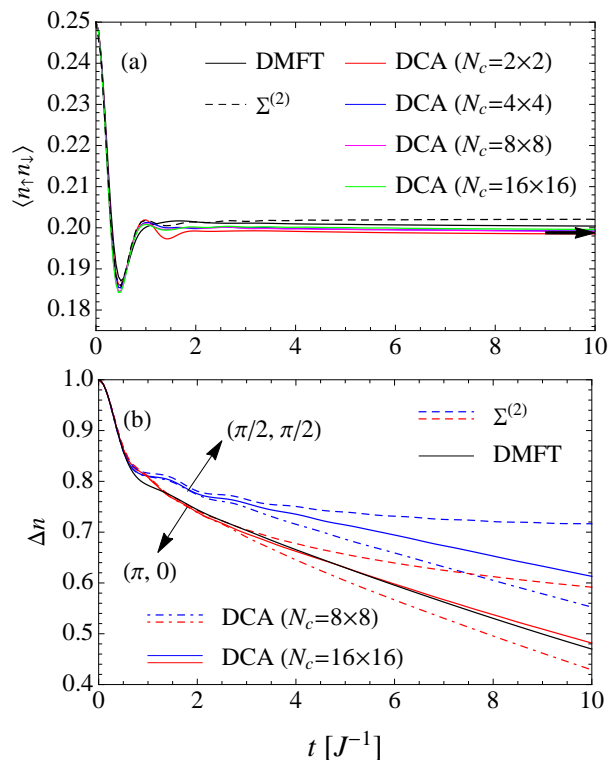


FIG. 4: (a) The double occupancy and (b) the jump in the momentum distribution for a quench $U/J = 0 \rightarrow 2$ in the 2D Hubbard model, obtained by DCA with the average of cluster types A and B, as compared with other methods. The arrow in (a) indicates the thermal value evaluated from DCA with $N_c = 16 \times 16$.

that the double occupancy takes, fairly soon after the quench, a value close to the thermal value [arrows in Figs. 1(a) and 2(a)]. For integrable models, nonequilibrium states are often described by the generalized Gibbs ensemble⁵⁴ in terms of a macroscopic number of integrals of motion. Our analysis suggests that $d(t)$ is not very sensitive to the nontrivial conserved quantities of the Hubbard model,⁵⁵ and that the total energy along with the total number of particles almost fully describes the stationary value of $d(t)$.

IV. INTERACTION QUENCH - 2D HUBBARD MODEL

Now let us turn to the interaction quench in the 2D Hubbard model, and investigate whether there is a qualitative change in the relaxation dynamics when going from 1D to 2D. In Fig. 4, we plot the time evolution for $d(t)$ and $\Delta n(t)$ for 2D. Since the cluster types A and B give quantitatively similar results, we take the average of cluster types A and B in the results of DCA to accelerate the convergence with respect to N_c , as we did for 1D. We can see that $d(t)$ quickly relaxes to the thermal value [an arrow in Fig. 4(a)] without generating long-lived oscillations. This is similar to the infinite-dimensional case. For $d(t)$, we find that the dependence on N_c is quite small (with DMFT already providing a good estimate), which implies that the nonlocal correlations are less relevant for local

quantities in 2D.

However, if we turn to $\Delta n(t)$ which is a nonlocal quantity, we immediately notice that $\Delta n(t)$ now dramatically depends on the position along the Fermi surface [while DMFT only gives a momentum-independent $\Delta n(t)$]. Note that the DCA results do converge with respect to N_c in the short-time regime up to $tJ \lesssim 2$, where the momentum dependence already starts to grow. In the plot we have focused on the nodal $(\pi/2, \pi/2)$ and antinodal $(\pi, 0)$ points, and we consider clusters up to $N_c = 16 \times 16$ (since we need $N_c \geq 4 \times 4$ to distinguish the nodal and antinodal sectors). As was the case in 1D, $\Delta n(t)$ is sensitive to N_c , and even with clusters as large as $N_c = 16 \times 16$ we still have a finite cluster-size effect. It seems that DCA+IPT is approaching $\Sigma^{(2)}$ in the large N_c limit (at least for Δn) in this interaction range. At present, going to larger clusters is technically difficult due to memory limitations, since we have to keep N/N_c large enough (in Fig. 4 we take $N = 256 \times 256$).

A salient feature in Fig. 4(b) is that, while $\Delta n(t)$ evolves completely uniformly over the momentum space in the early stage ($tJ \leq 0.5$), it suddenly starts to exhibit a momentum dependence after that period: The antinodal point $(\pi, 0)$ relaxes faster than the nodal point $(\pi/2, \pi/2)$, where a slowly damped oscillation appears in the time evolution. The latter is reminiscent of the 1D results. The DCA simulation suggests that the momentum distribution eventually reaches the thermal distribution with $\Delta n = 0$. If one goes to larger U , the momentum variation of $\Delta n(t)$ is weakened.

Now, let us examine what the momentum-dependent relaxation seen in $\Delta n(t)$ implies, based on the quasiparticle picture, which is valid in the weak-interaction regime. The lifetime $\tau(\mathbf{k})$ of the quasiparticle with energy ω can be evaluated from the equilibrium retarded self-energy,⁵⁶

$$\tau(\mathbf{k})^{-1} = 2\text{Im}\Sigma^R(\mathbf{k}, \omega).$$

The 2D Hubbard model on the square lattice at half filling is special, since the one-particle dispersion has a van Hove singularity right at the Fermi energy ϵ_F . This makes the density of states diverging logarithmically, and the system behaves as a ‘‘marginal Fermi liquid,’’ i.e., $\text{Im}\Sigma^R(\mathbf{k}, \omega) \propto \omega$ around $\omega = \epsilon_F$.⁵⁷ In the top panel of Fig. 5, we plot $\text{Im}\Sigma^R(\mathbf{k}, \omega)$ obtained from $\Sigma^{(2)}$. Even in the weak-coupling regime, $\text{Im}\Sigma^R(\mathbf{k}, \omega)$ is highly anisotropic in momentum space: It is peaked at $(\pi, 0)$, while $(\pi/2, \pi/2)$ exhibits a saddle-point behavior. In the bottom panel of Fig. 5, we compare the inverse quasiparticle lifetime $\text{Im}\Sigma^R(\mathbf{k}, \omega)$ with the relaxation rate γ for Δn . The latter is evaluated by fitting the DCA result for $\Delta n(t)$ [Fig. 4(b)] with a single exponential $Ae^{-\gamma t}$. We find that the momentum dependence of γ (whose qualitative tendency is independent of N_c) is well reproduced by $\text{Im}\Sigma^R(\mathbf{k}, \omega)$. This suggests that the momentum-dependent relaxation of $\Delta n(t)$ is in fact governed by the quasiparticles, which have a longer lifetime at $(\pi/2, \pi/2)$.

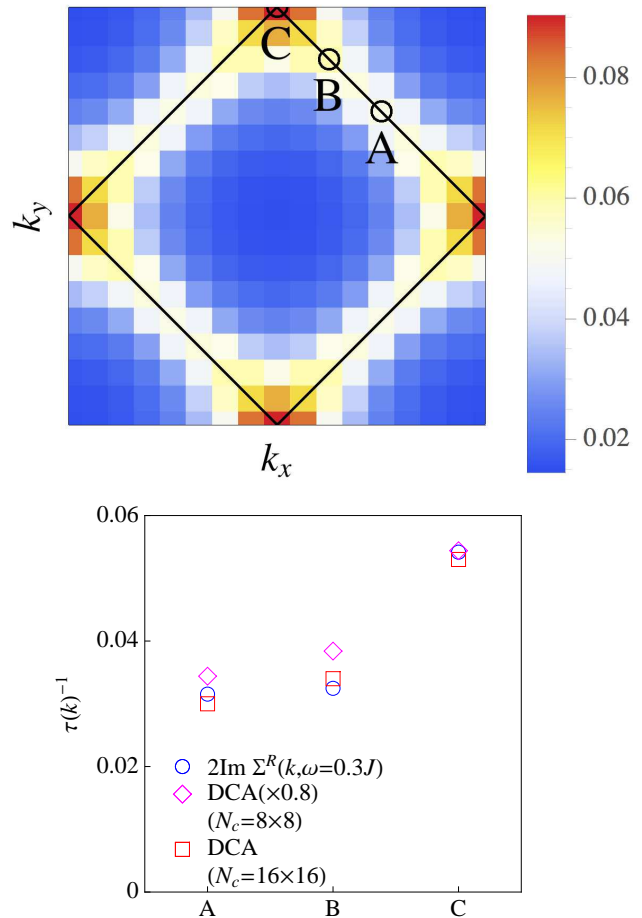


FIG. 5: (Color online) Top: Color-coded plot of $|\text{Im}\Sigma^R(\mathbf{k}, \omega)/\omega|$ at $\omega = 0.3J$ for $U/J = 2$ and $T = 0$. Solid lines indicate the noninteracting Fermi surface. Bottom: Inverse of the quasiparticle lifetime $\tau(\mathbf{k})$ estimated with the nonequilibrium DCA, along with that estimated from $\text{Im}\Sigma^R(\mathbf{k}, \omega)$ for three positions (A, B, and C on the left panel) in the Brillouin zone.

V. 2D HUBBARD MODEL DRIVEN BY DC FIELDS

The nonequilibrium DCA proposed here is a general framework, which allows to study not only nonequilibrium phenomena resulting from interaction quenches but also those induced by dc-field quenches. Let us demonstrate this here for the 2D Hubbard model on the square lattice driven by a dc electric field E . The field is introduced by the Peierls substitution $\epsilon(\mathbf{k}) \rightarrow \epsilon(\mathbf{k} - \mathbf{A}(t))$ in the noninteracting part of the lattice Hamiltonian with $\mathbf{A}(t) = -\mathbf{E}t$ the vector potential, where the field is taken to be along the diagonal direction, i.e., $\mathbf{E} = E(1, 1)$. We switch on the field at $t = 0$ with the initial state being the noninteracting one at zero temperature. The interaction is quenched as $U/J = 0 \rightarrow 2$ at the same time as the field is turned on at $t = 0$. A physical observable of interest in this situation is the current,

$$j = -i \sum_{k\sigma} v_{k-A(t)} G_{k\sigma}^{\text{lat}, <}(t, t),$$

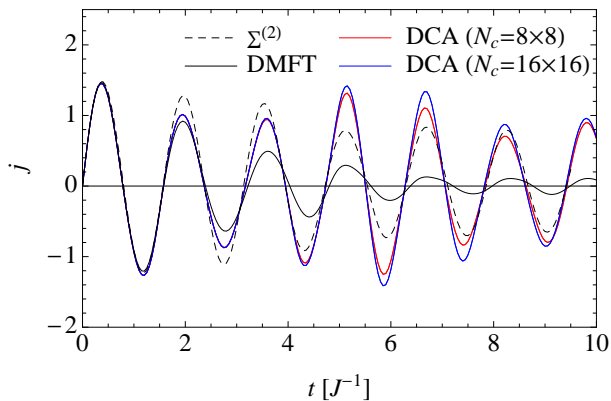


FIG. 6: The current in the 2D Hubbard model driven by a dc electric field $E = 4$ obtained with DCA for $N_c = 8 \times 8, 16 \times 16$ (red and blue curves, respectively) and with $\Sigma^{(2)}$ (dashed curve). The cluster type dependence (A or B) is negligible.

where $v_k = \sum_i \partial \epsilon_k / \partial k_i$ is the velocity along the $(1, 1)$ direction.

In Fig. 6, we plot the current obtained with DCA for $N_c = 8 \times 8, 16 \times 16$ and with $\Sigma^{(2)}$. Here, both the cluster types A and B in DCA give almost the same results for these N_c . By comparing the results for $N_c = 8 \times 8$ and $N_c = 16 \times 16$, we can confirm that the current converges well with respect to N_c up to $tJ \lesssim 5$, which implies that the DCA results can be considered as representative of the thermodynamic limit within this time domain.

One can see that the current shows a coherent Bloch oscillation with frequency $E = 4$, but an important question is its damping. DMFT predicts a rapid damping of the Bloch oscillation, which is consistent with the previous study of the dc-field problem for the Hubbard model.⁵⁸ On the other hand, as we take account of the momentum dependence of the self-energy in DCA or in $\Sigma^{(2)}$, we see a clear difference in the behavior of the oscillation between DCA and $\Sigma^{(2)}$: In the DCA case, the current exhibits a longer-lived behavior with a beating, i.e., the amplitude of the oscillation oscillates with a longer period, while in the $\Sigma^{(2)}$ case, the current is damped monotonically. This in itself is physically interesting, and also shows that DCA combined with the IPT cluster solver is not equivalent to $\Sigma^{(2)}$, even in the limit of $N_c \rightarrow \infty$. DCA can provide more reliable results than $\Sigma^{(2)}$ because the formalism allows one to check the convergence with N_c . The difference in the results between DCA and $\Sigma^{(2)}$ comes from the fact that DCA imposes a self-consistency condition which provides a feedback from the lattice solution to the cluster, whereas $\Sigma^{(2)}$ does not. If one keeps N/N_c large enough while taking the limit of $N_c \rightarrow \infty$ and $N \rightarrow \infty$, the non-trivial effect of this self-consistency may survive.

Another advantage of DCA over $\Sigma^{(2)}$ is that there is room for improving the cluster solver for DCA, while it is numerically difficult to extend $\Sigma^{(2)}$ by considering higher-order diagrams for the self-energy with a large number of k points. In practice, the second-order is the highest for which lattice

perturbation theory can be implemented in nonequilibrium.

VI. SUMMARY

We have formulated the nonequilibrium dynamical cluster theory, which enables one to investigate the effects of non-local spatial correlations on nonequilibrium many-body systems by systematically changing the cluster size. We have applied the method to the interaction-quench problem for the Hubbard model in one and two dimensions, and found a peculiar *momentum-dependent relaxation* of quasiparticles in 2D. This should be experimentally observable by means of time-resolved ARPES measurements, and such experiments may open an interesting avenue for probing marginal Fermi liquids in nonequilibrium. We have also applied the method to the Hubbard model driven by a dc electric field, and found an enhancement of the Bloch oscillations, compared to the result predicted by DMFT.

Benchmark calculations in 1D revealed a good convergence for local properties, while the accuracy of non-local quantities is limited due to our perturbative solution of the impurity problem. Therefore, it will be important to test the cluster approach by also using alternative nonequilibrium impurity solvers, such as NCA in the strong-coupling regime,³⁹ or quantum Monte Carlo (QMC) solvers on smaller clusters in the weak-coupling regime.³⁸ While these cluster solvers cannot access large cluster sizes, such as our $N_c = 16 \times 16$ for the 2D Hubbard model, due to the exponentially scaling computational cost, for local and quasilocal quantities such as nearest-neighbor correlation functions the cluster-size dependence can be eliminated even with small clusters. For example, one may be able to reach $N_c = 8$ with the QMC solver or $N_c = 4$ with the NCA solver. The $N_c = 8$ cluster can distinguish the nodal [$k = (\pi/2, \pi/2)$] and antinodal [$(\pi, 0)$ and $(0, \pi)$] sectors, where the momentum-dependent relaxation is most evidently observed. An interesting prospect of the cluster method combined with weak-coupling perturbation theory will be the simulation of the real-time dynamics of systems with long-range order (e.g. d -wave superconductivity or charge density waves), which would be inaccessible by lattice perturbation theories.

Acknowledgments

The calculations were carried out on the UniFr cluster and the Perseus computer cluster of the University of Geneva financed by “Fondation Ernst et Lucie Schmidheiny”. The DMRG simulations employed the ALPS libraries.^{59,60} N.T. was supported by a Grant-in-Aid for Scientific Research on Innovative Areas “Materials Design through Computics: Complex Correlation and Non-equilibrium Dynamics” (Grant No. 25104709), and another for Young Scientists (B) (Grant No. 25800192) from MEXT, and SNF Grant No. PP0022-118866. H.A. is supported by a MEXT Grant No. 26247057. P.W. acknowledges support from FP7 ERC Starting Grant No. 278023.

- ¹ A. Polkovnikov, K. Sengupta, A. Silva, and M. Vengalattore, *Rev. Mod. Phys.* **83**, 863 (2011).
- ² A. Daley, C. Kollath, U. Schollwöck, and G. Vidal, *J. Stat. Mech.: Theor. Exp.* **2004**, P04005 (2004).
- ³ S. White and A. Feiguin, *Phys. Rev. Lett.* **93**, 076401 (2004).
- ⁴ U. Schollwöck, *Rev. Mod. Phys.* **77**, 259 (2005).
- ⁵ W. Metzner and D. Vollhardt, *Phys. Rev. Lett.* **62**, 324 (1989).
- ⁶ A. Georges, G. Kotliar, W. Krauth, and M. J. Rozenberg, *Rev. Mod. Phys.* **68**, 13 (1996).
- ⁷ P. Schmidt and H. Monien, arXiv:cond-mat/0202046.
- ⁸ J. K. Freericks, V. M. Turkowski, and V. Zlatić, *Phys. Rev. Lett.* **97**, 266408 (2006).
- ⁹ H. Aoki, N. Tsuji, M. Eckstein, M. Kollar, T. Oka, and P. Werner, *Rev. Mod. Phys.* **86**, 779 (2014).
- ¹⁰ L. Perfetti, P. A. Loukakos, M. Lisowski, U. Bovensiepen, H. Eisaki, and M. Wolf, *Phys. Rev. Lett.* **99**, 197001 (2007).
- ¹¹ F. Schmitt, P. S. Kirchmann, U. Bovensiepen, R. G. Moore, L. Rettig, M. Krenz, J.-H. Chu, N. Ru, L. Perfetti, D. H. Lu, et al., *Science* **321**, 1649 (2008).
- ¹² J. Graf, C. Jozwiak, C. L. Smallwood, H. Eisaki, R. A. Kaindl, D.-H. Lee, and A. Lanzara, *Nat. Phys.* **7**, 805 (2011).
- ¹³ R. Cortés, L. Rettig, Y. Yoshida, H. Eisaki, M. Wolf, and U. Bovensiepen, *Phys. Rev. Lett.* **107**, 097002 (2011).
- ¹⁴ C. L. Smallwood, J. P. Hinton, C. Jozwiak, W. Zhang, J. D. Koralek, H. Eisaki, D.-H. Lee, J. Orenstein, and A. Lanzara, *Science* **336**, 1137 (2012).
- ¹⁵ T. Maier, M. Jarrell, T. Pruschke, and M. H. Hettler, *Rev. Mod. Phys.* **77**, 1027 (2005).
- ¹⁶ M. Greiner, O. Mandel, and T.W. Hänsch, and I. Bloch, *Nature (London)* **419**, 51 (2002).
- ¹⁷ D. Chen, M. White, C. Borries, and B. DeMarco, *Phys. Rev. Lett.* **106**, 235304 (2011).
- ¹⁸ S. Trotzky, Y.-A. Chen, A. Flesch, I. P. McCulloch, U. Schollwöck, J. Eisert, and I. Bloch, *Nat. Phys.* **8**, 325 (2012).
- ¹⁹ M. Cheneau, P. Barmettler, D. Poletti, M. Endres, P. Schauß, T. Fukuhara, C. Gross, I. Bloch, C. Kollath, and S. Kuhr, *Nature (London)* **481**, 484 (2012).
- ²⁰ C. Kollath, A. M. Läuchli, and E. Altman, *Phys. Rev. Lett.* **98**, 180601 (2007).
- ²¹ S. R. Manmana, S. Wessel, R. M. Noack, and A. Muramatsu, *Phys. Rev. Lett.* **98**, 210405 (2007).
- ²² M. Moeckel and S. Kehrein, *Phys. Rev. Lett.* **100**, 175702 (2008).
- ²³ M. Eckstein, M. Kollar, and P. Werner, *Phys. Rev. Lett.* **103**, 056403 (2009).
- ²⁴ P. Barmettler, M. Punk, V. Gritsev, E. Demler, and E. Altman, *Phys. Rev. Lett.* **102**, 130603 (2009).
- ²⁵ C. Karrasch, J. Rentrop, D. Schuricht, and V. Meden, *Phys. Rev. Lett.* **109**, 126406 (2012).
- ²⁶ P. Werner, N. Tsuji, and M. Eckstein, *Phys. Rev. B* **86**, 205101 (2012).
- ²⁷ S. A. Hamerla and G. S. Uhrig, *Phys. Rev. B* **87**, 064304 (2013).
- ²⁸ N. Tsuji, M. Eckstein, and P. Werner, *Phys. Rev. Lett.* **110**, 136404 (2013).
- ²⁹ S. A. Hamerla and G. S. Uhrig, *Phys. Rev. B* **89**, 104301 (2014).
- ³⁰ J. Berges, S. Borsányi, and C. Wetterich, *Phys. Rev. Lett.* **93**, 142002 (2004).
- ³¹ A. I. Lichtenstein and M. I. Katsnelson, *Phys. Rev. B* **62**, R9283 (2000).
- ³² G. Kotliar, S. Y. Savrasov, G. Pálsson, and G. Biroli, *Phys. Rev. Lett.* **87**, 186401 (2001).
- ³³ M. H. Hettler, A. N. Tahvildar-Zadeh, M. Jarrell, T. Pruschke, and H. R. Krishnamurthy, *Phys. Rev. B* **58**, R7475 (1998).
- ³⁴ M. H. Hettler, M. Mukherjee, M. Jarrell, and H. R. Krishnamurthy, *Phys. Rev. B* **61**, 12739 (2000).
- ³⁵ J. Rammer, *Quantum Field Theory of Non-equilibrium States* (Cambridge University Press, Cambridge, 2007).
- ³⁶ M. Eckstein, M. Kollar, and P. Werner, *Phys. Rev. B* **81**, 115131 (2010).
- ³⁷ N. Tsuji and P. Werner, *Phys. Rev. B* **88**, 165115 (2013).
- ³⁸ P. Werner, T. Oka, and A. J. Millis, *Phys. Rev. B* **79**, 035320 (2009).
- ³⁹ M. Eckstein and P. Werner, *Phys. Rev. B* **82**, 115115 (2010).
- ⁴⁰ E. Arrigoni, M. Knap, and W. von der Linden, *Phys. Rev. Lett.* **110**, 086403 (2013).
- ⁴¹ C. Gramsch, K. Balzer, M. Eckstein, and M. Kollar, arXiv:1306.6315.
- ⁴² M. Balzer and M. Potthoff, *Phys. Rev. B* **83**, 195132 (2011).
- ⁴³ M. Knap, W. von der Linden, and E. Arrigoni, *Phys. Rev. B* **84**, 115145 (2011).
- ⁴⁴ M. Balzer, N. Gdaniec, and M. Potthoff, *J. Phys.: Condens. Matter* **24**, 035603 (2012).
- ⁴⁵ C. Jung, A. Lieder, S. Brener, H. Hafermann, B. Baxevanis, A. Chudnovskiy, A. Rubtsov, M. Katsnelson, and A. Lichtenstein, *Ann. Phys.* **524**, 49 (2012).
- ⁴⁶ E. Muñoz, C. J. Bolech, and S. Kirchner, *Phys. Rev. Lett.* **110**, 016601 (2013).
- ⁴⁷ G. Vidal, *Phys. Rev. Lett.* **98**, 70201 (2007).
- ⁴⁸ I. P. McCulloch, arXiv:0804.2509.
- ⁴⁹ F. Verstraete, J. García-Ripoll, and J. Cirac, *Phys. Rev. Lett.* **93**, 207204 (2004).
- ⁵⁰ M. Zwolak and G. Vidal, *Phys. Rev. Lett.* **93**, 207205 (2004).
- ⁵¹ A. E. Feiguin and S. R. White, *Phys. Rev. B* **72**, 220401 (2005).
- ⁵² M. Kollar, F. A. Wolf, and M. Eckstein, *Phys. Rev. B* **84**, 054304 (2011).
- ⁵³ E. H. Lieb and F. Y. Wu, *Phys. Rev. Lett.* **20**, 1445 (1968).
- ⁵⁴ M. Rigol, V. Dunjko, V. Yurovsky, and M. Olshanii, *Phys. Rev. Lett.* **98**, 050405 (2007).
- ⁵⁵ B. Shastri, *Phys. Rev. Lett.* **56**, 1529 (1986).
- ⁵⁶ C. Hodges, H. Smith, and J. W. Wilkins, *Phys. Rev. B* **4**, 302 (1971).
- ⁵⁷ P. C. Pattnaik, C. L. Kane, D. M. Newns, and C. C. Tsuei, *Phys. Rev. B* **45**, 5714 (1992).
- ⁵⁸ M. Eckstein and P. Werner, *Phys. Rev. Lett.* **107**, 186406 (2011).
- ⁵⁹ A. Albuquerque, F. Alet, P. Corboz, P. Dayal, A. Feiguin, S. Fuchs, L. Gamper, E. Gull, S. Gürtler, A. Honecker, et al., *J. Mag. Mag. Mater.* **310**, 1187 (2007).
- ⁶⁰ B. Bauer, L. D. Carr, H. G. Evertz, A. Feiguin, J. Freire, S. Fuchs, L. Gamper, J. Gukelberger, E. Gull, S. Guertler, et al., *J. Stat. Mech.: Theor. Exp.* **2011**, P05001 (2011).